JOURNAL OF MATERIALS SCIENCE **36** (2001) 1183–1188

Study of the containerless undercooling of Ti-Ce immiscible alloys

T. J. RATHZ
University of Alabama in Huntsville, Huntsville, Alabama, 35899, USA
E-mail: tom.rathz@msfc.nasa.gov

M. B. ROBINSON
NASA/Marshall Space Flight Center, Huntsville, Alabama, 35812, USA

D. LI
Nicol Hall, Queen's University, Kingston, Canada

G. L. WORKMAN, G. WILLIAMS
University of Alabama in Huntsville, Huntsville, Alabama, 35899, USA

Ti-Ce immiscible alloys of compositions across the miscibility gap were containerlessly processed in both a low-gravity and a unit-gravity environment. Although undercooling of the single-phase liquid into the miscibility gap could not be observed, undercooling did occur across the miscibility gap for the separated liquid Ti-rich phase. The low gravity, quiescent environment favored higher undercooling over the unit-gravity samples. Every undercooled sample had massive separation of the liquid phases. Metallurgical analysis of samples undercooled in unit-gravity showed signs of vigorous convective stirring and shearing of the L_1 Ti-liquid by the applied levitation electromagnetic field. In low-gravity processed samples, the L_1 liquid formed a near-concentric sphere within a Ce shell with some residual smaller spherical particles dispersed throughout the Ce. This configuration is predicted from wetting theory and from Marangoni separation. Plots of both the melting and solidification temperatures indicate that the monotectic temperature is $1831 \pm 12^{\circ}$K rather than the 1723°K as reported in the literature. From chemical and diffraction analysis, the solubility of Ce in the Ti-rich phase was found to be extended; also, some cerium oxide precipitates formed but no perceptible dissolved oxygen within the Ce or Ti phases was found which indicates that the higher monotectic temperature reported here is probably not an oxygen effect.

1. Introduction

Solidification of hypermonotectic systems is of industrial importance for the formation of in-situ composite microstructures. However, because of the various liquid-liquid separation mechanisms that can lead to gross segregation, many solidification studies have been performed to understand the relative importance and, hopefully, to the control of these mechanisms. When cooling through the immiscibility domes of stable monotectic systems containing liquid L_1 and L_2 of the higher and lower melting temperature elements, respectively, the initial separation mechanism that occurs on the surface of the sample can be of critical importance in the subsequent bulk separation and solidification morphology. This liquid surface separation can be a barrier-less nucleation process as opposed to the liquid-to-solid nucleation process.

Previous tests of classical nucleation theory applied to liquid-liquid gap miscibility systems found a discrepancy between experiment and theory in the ability to undercool either of the *liquids* before the L_1-L_2 separated [1, 2]. To model this initial separation process, free-energy gradient [3] and density gradient [4] theories have been put forth. If there is a large enough interaction between the critical liquid and the crucible, both models predict a wetting temperature (T_w) above which the minority liquid perfectly wets and forms *layers* at the crucible interface, but only on one side of the immiscibility dome. Materials with compositions on the other side of the dome will have simple surface adsorption by the minority liquid before bulk separation occurs when the coexistence line is reached. If the interaction between the critical liquid and the crucible were to decrease, T_w would increase, eventually approaching the critical consolute temperature (T_{cc}). At this point, large composition ranges would exist in which non-perfect wetting conditions prevail, resulting in undercooling of the liquid-phase separation event across the miscibility gap. The contra-positive of this argument has recently been demonstrated in a metastable immiscible system [5] using different oxide layers as crucibles. The bulk fluid flows and resulting microstructure will

then depend on what has happened at the surface and the subsequent processing conditions.

In the past several decades, many experiments in space [6–8] have been performed on liquid metal binary immiscible systems for the purpose of reducing gravity driven separation mechanisms and to highlight the effects that crucibles of different materials may have on the wetting/separation process of the liquids. Several other studies have been performed on immiscibles in a semi-container environment using an emulsion technique [9, 10]. Only one previous study on stable immiscible systems was performed using a completely containerless processing technique [11] and the results of that investigation are similar to the emulsion studies. In all cases, surface wetting was blamed as the cause for the similar microstructures or the asymmetry in the ability to undercool the liquid below the binoidal on one side of the immiscibility dome.

Containerless processing eliminates external nucleants that prevent undercooling and the removal of a large source of contamination that a container provides for these reactive materials. By removing the container completely, the loss of the crucible/liquid interaction should produce a shift in T_w and thus change the wetting characteristics at the surface. A change in the liquid wetting potential at the surface of a containerless droplet should change the nucleation and separation behavior of the droplet. By varying the amounts of undercooling and subsequent solidification speeds allow assorted amounts of separation of the two liquid phases to occur before complete solidification occurs. In this study, we attempt to determine the amount of undercooling that either the surface liquid-liquid (imperfect wetting) or bulk liquid-solid undergo across the miscibility gap composition range by monitoring the temperature of the sample with optical pyrometry. Another purpose of this study is to examine the effects of weightlessness on the separation process of the immiscible liquids. Microstructural analysis will correlate the degree of undercooling and the separation mechanisms involved.

2. Experimental details

The Ti-Ce alloys were prepared at the Materials Preparation Center of Ames Laboratory, USDOE. The phase diagram is given in Fig. 1. Seven compositions were used which ranged between 46.8 and 92.0 w/o Ce with purity levels averaging 99.9 w/o. The average standard deviation of each composition was ±0.2 w/o. The masses of the samples ranged between 0.34 to 0.43 grams. The uncertainty of the alloy density gave calculated, ideally spherical sample diameters of 5.3 ± 0.2 mm. Raw samples were opened and stored under inert gas and remained in the evacuated or gas-filled processing chamber at all times. Oxygen and nitrogen levels within the samples before and after processing are given in Table I.

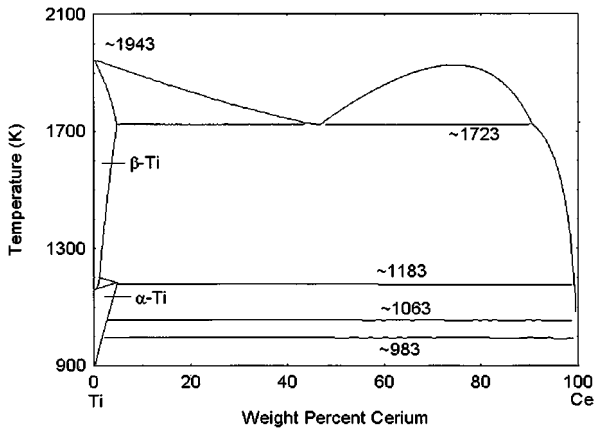

Figure 1 Binary phase diagram of the monotectic Ti-Ce system [14].

TABLE I Chemical composition of the Ce component

Most Important Impurities (%)									
Fe	Ca	Mg	Cu	Ta	Si	N	O	Purity (%)	Ref
0.002	Tr	Tr	Tr	--	--	--	--	99	17
0.02	0.03	0.02	--	0.05	0.03	(←	0.2)	99.8	17, 19
0.004	Tr	Tr	0.005	0.001	0.001	0.01	0.02	99.95	*
						0.02	0.06		**

* This study before processing (Ames analysis).
** This study after processing (LECO analysis).

For measurements of the amount of undercooling associated with the liquid-to-solid transformation, the equilibrium monotectic transition temperature (T_m) had to be known from which the amount of undercooling underwent by the β-Ti liquid phase could be measured. Depending on the amount of undercooling that a liquid undergoes, a nucleation event will trigger a fraction of the liquid to rapidly and nearly adiabatically solidify [12]. This rapid release of the latent heat (recalescence) will cause the remaining liquid to quickly attain the equilibrium melting temperature for that phase whereupon the remaining liquid will solidify at a rate determined by the heat extraction capability of the process. In this study, we use both the melting temperature upon heating and the recalescence peak temperature (T_p) upon cooling to determine the monotectic temperature.

2.1. Low-gravity process

The 105-meter Drop Tube Facility at NASA/Marshall Space Flight Center [13] was used to provide low-gravity (hereafter labeled 0-g), containerless conditions. This facility is 105 m in length and 26.6 cm in diameter. Initial vacuum levels in the Drop Tube were $\sim 6 \times 10^{-5}$ Pa and the leak rate over a typical 7-hour work period was $\sim 3 \times 10^{-7}$ Pa/hr. The Tube was backfilled with Ti-gettered and 10 μm filtered, 5-nines pure He-6%H_2 gas to a pressure of 89.5 kPa. The 0-g samples were processed by electromagnetic (EM) levitation and heating at a frequency of 450 kHz. The coil arrangement consisted of a single, 7-turn lower and 2-turn serially opposed upper coil operating at 190 amps. Once the sample was molten and heated into the single solution region at a temperature of 2023°K, the power to the coil was automatically turned off and the material allowed to free-fall. At 89.5 kPa pressure, total solidification of the L_2 Ce-rich liquid could occur during free-fall; however, this pressure generated a calculated drag force of

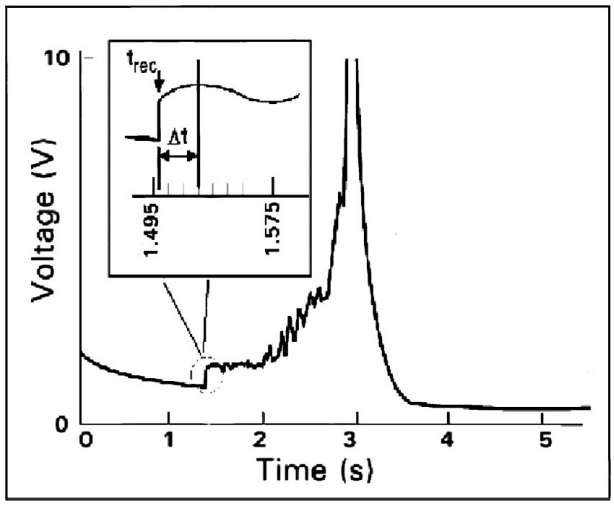

Figure 2 A typical silicon detector voltage curve of a 0-g sample falling down the Drop Tube. The recalescence event (circled) is followed by reflections from the Drop Tube wall or other optics. The inset curve is a magnification of the recalescence from which the recalescence time, t_{rec}, and the solidification time, Δt, can be determined.

25 milli-g's on the sample. At the bottom of the Drop Tube, the samples were funneled onto a 1–1/2 inch diameter butterfly vacuum valve where they cooled before opening the valve and allowing the sample to roll directly into a thick-walled Pyrex tube where they were then flame sealed.

An eight channel, 1.25 MHz per channel, 12-bit resolution data acquisition unit was used to monitor silicon detector voltages generated by the brightness of the falling sample. Fig. 2 is a typical detector trace showing a recalescence at time, $t_{rec} = 1.49$ seconds followed by reflection peaks. The signal saturates as the samples passes by the detector and then quickly falls to background levels. The inset curve shows a magnified view of the recalescence from which a more precise t_{rec} and an apparent time to solidify, Δt, can be obtained. Time resolution was 5 μs over the 5.2 seconds of total time it took for a sample to drop through the gaseous environment of the Drop Tube. The temperature at which recalescence occurred (i.e., the amount of undercooling) was calculated by knowing T_m and from the difference between the final time (t_{rec}) at which recalescence began and the amount of time it took to get to T_m. The cooling model assumed the sample to consist entirely of only the composition of the outer separated liquid phase (L_2); the Rule of Mixtures was used to obtain a 90 w/o Ce solution value of the heat capacity, density, and emissivity. Release temperatures for all compositions were kept to 2023°K–100 degrees above the published critical consolute temperature (T_{cc}). This temperature would place the alloy in the single-solution region from which any surface wetting effects could be observed.

2.2. Unit-gravity process

Unit-gravity studies were performed atop the Drop Tube Facility in the same EM coil that was used to process the 0-g samples. The samples were levitated and heated to 2023°K at which temperature a cooling gas was applied. Six-nines pure, liquid-nitrogen trapped, non-gettered, non-filtered He-6%H_2 gas was used. Since the samples could not be totally solidified in the EM coil due to the heating produced by the EM levitation field, the samples were cooled below the range of the pyrometer (~1573°K) and then released down the Tube to cool and solidify the remaining L2 Ce-rich liquid. The samples at the bottom of the Drop Tube were retrieved in the same manner as described for the 0-g samples. For both the 0-g and 1-g studies, an Ircon Modline two-color pyrometer was used to measure the sample temperature in the EM coil at a rate of 100 readings per second and an accuracy of 1%. The melting temperatures of 3-nines pure Zr and Ti were used as pyrometer calibration standards.

The processed samples were always kept in an evacuated dessicator between hot mounting, grinding, polishing, or electron microprobing. The final polishing technique used 0.04 μm silicon dioxide solution on a porous synthetic cloth for 2 minutes at 15 Newton force. Optical photographs were taken immediately after polishing at 16, 100, and 200 magnifications. A JEOL model JXA8900 electron microprobe having a beam diameter of ~1 μm and employing wavelength dispersive analysis (WDS) was used for the quantitative microstructural analysis. A 4-nines pure Ti and a 3-nines pure Ce specimen mounted and polished in the same manner as the alloys were used as WDS calibration standards.

3. Results and discussion

3.1. Temperature measurements

Measurements were performed first for the 1-g samples in the EM coil. A typical heating/cooling curve is presented in Fig. 3. For the 36 1-g samples measured, the monotectic temperature, T_m, was determined from the melting isotherm and from the recalescence peak temperature (T_p) as 1833 ± 19°K. The melt temperature during heating of the 0-g Drop Tube processed samples was also used to determine T_m. For the 34 0-g samples that were dropped, T_m was measured only during heating at the melt plateau as 1830 ± 17°K. The consistent melt plateau for 0- and 1-g samples implied that the as-cast materials from Ames Laboratories had separated and solidified with a monotectic structure that was also

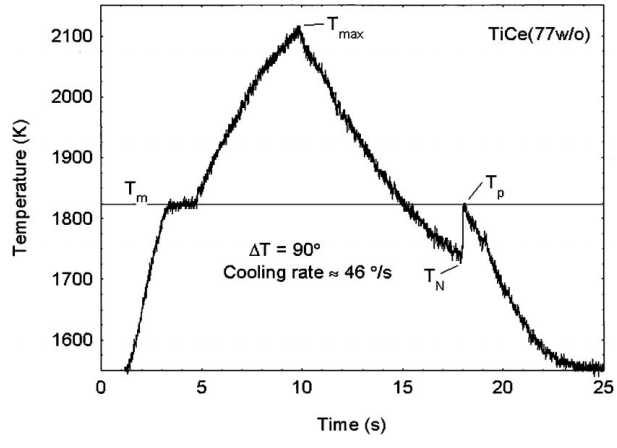

Figure 3 Typical heating/cooling curve in the EM coil. T_m is the monotectic, T_p is the recalescence peak, T_N is the nucleation temperature, and T_{max} is the maximum temperature.

determined metallographically. The average T_m of this study differs significantly from the reported literature value of 1723°K [14]. Over the period of time to perform this entire study, 61 3-nines pure Zr and 23 3-nines Ti drops (6 mm diameter) were used as melting point calibrations for the optical pyrometer. The pyrometer had a systematic error of 11 ± 16 above and 1 ± 5 degrees below the Zr and and Ti melting temperatures, respectively. Because of the narrow separation of the wavelength ranges of the detectors of the pyrometer, the pyrometer's linearity, and the close proximity of the Ti, Zr, and Ce spectral emissivity values [15], the Zr and Ti melting temperatures were used with confidence as calibrations for the measured alloy temperatures. Any changes in the emissivity due to slight oxidation of the surface should have negligible temperature measurement effects due to the 2-color signal ratio of the pyrometer. No patches of oxide were observed floating on the surface during the entire process. There was, however, about 400 ppm O_2 absorbed during the processing of the Ti-Ce in this study, most of which might be accountable in the slight cerium oxide precipitate.

Previous Ti-Ce phase diagram studies [16–19] had different results. Taylor [18] found T_m to be around 1603°K and Ce solubility in β-Ti to be about 0.8 w/o while Savitskii and Burkhanov [17] found solubility about 5 times greater and a T_m around 1723°K; however, Murray reports a solubility of ∼5 w/o [16]. The major impurities found in the Ce used in each study are given in Table I. Taylor gives no amount for the oxygen or nitrogen contents of his study whereas Saviskii [19] gives a combined total of less than 0.2%; this study also found these gases as the major source of contamination but at a lower level than the previous studies. The oxygen content of materials used in previous studies [19] were an order of magnitude greater than this study suggesting that some inaccuracies in the published phase diagrams may be due to the effects of oxygen as suggested by Murray.

Fig. 4 shows the amount of undercooling undertaken by L_1 across the miscibility gap of the Ti-Ce phase diagram before the β-Ti and L_2 transformation. The monotectic line and the binoidal curve have been shifted to account for the measured T_m. From Fig. 4, it can be seen that the samples containerlessly processed in the 0-g environment of the Drop Tube typically undercooled more than those in 1-g. The discrepancy between the 1-g undercoolings and the 0-g undercoolings may be attributable to several factors. The stirring by the EM field of the 1-g samples will coalescence the nucleated droplets much faster (∼20–50 mm/s [20]) into larger spheres than the Marangoni convection (∼2 mm/s [21]) that is prominent in the 0-g samples. Without forced convection in 0-g to hasten the coagulation of the droplets, the liquid-liquid dispersion is essentially a high temperature emulsion. As seen in previously studied emulsions [9, 10], the small size of the droplets provides isolation of the most active nucleants and thus allows the bulk of the remaining Ti-rich liquid to undercool much more. Thus, the longer the active nucleant can stay away from the coalescing Ti-rich liquid, the more undercooling attainable. Also, any additional length of time that the small Ti-rich droplets can remain uncoalesced within the Ce-rich liquid, the better the Ti will be gettered of oxygen since Ce is about 5 orders of magnitude lower than Ti in its equilibrium oxygen value [22]. This should reduce the formation of Ti oxide nucleants.

Another factor for the undercooling differences may be the 0-g temperatures being a calculated number that depends on the thermophysical properties of an alloy that are not well-known. Instead, the Rule of Mixtures was used to determine alloy properties from the constituents. Also, the elemental properties are known at the melting point but not in the undercooled state. A worse case analysis of the calculated undercoolings based on the combined uncertainties of these thermophysical properties (i.e., density, heat capacity, emissivity, and recalescence time) result in a 10% error. Even with this error, the trend in larger undercoolings in the 0-g samples is still significant.

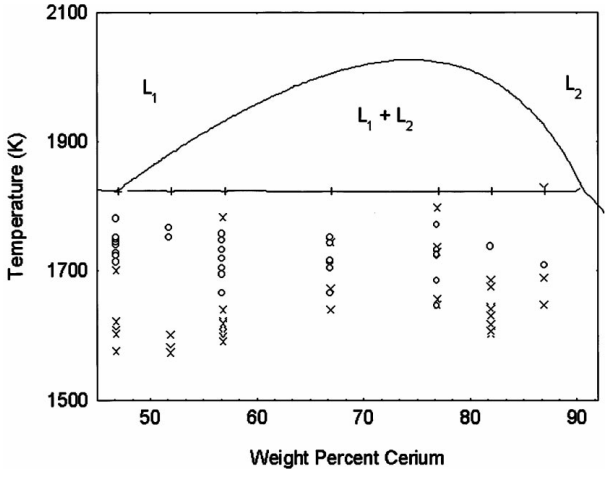

Figure 4 Immiscibility dome section of Fig. 1 showing a composite of all the undercooling measurements taken in this study. The Drop Tube data (X) shows significant undercooling over the EM coil data (O) despite large errors in the absolute calculated values. The monotectic line and the binoidal curve have been adjusted for the measured T_m values (+).

3.2. Microstructural results

All the samples were ground in half before polishing. Fig. 5a/5b and 5c/5d are representative of all the 0-g and 1-g specimens, respectively. Fig. 5a shows the Ti-rich liquid-phase that had separated and became spheres of various sizes. As expected, the size of the central, larger Ti sphere got smaller as the volume percent of the Ce-rich liquid increases. At all compositions, there was a Ce-rich layer as the outer shell of the sample whose thickness again depended on the initial volume fraction of Ce. Within the Ti spheres can be seen secondary separation of a Ce-rich phase into a random droplet morphology (Fig. 5b). X-ray diffraction analysis indicated that the only phases present were the α-Ti, Ce, and a very small amount of a form of cerium oxide.

No correlation of undercooling to the amount of dissolved Ce contained in the α-Ti could be made among the samples. However, the 1-g samples do have some differences to the 0-g samples. Using microprobe analysis, the average composition of the α-Ti phase for the 0-g samples was 7 ± 2 and that for the 1-g samples

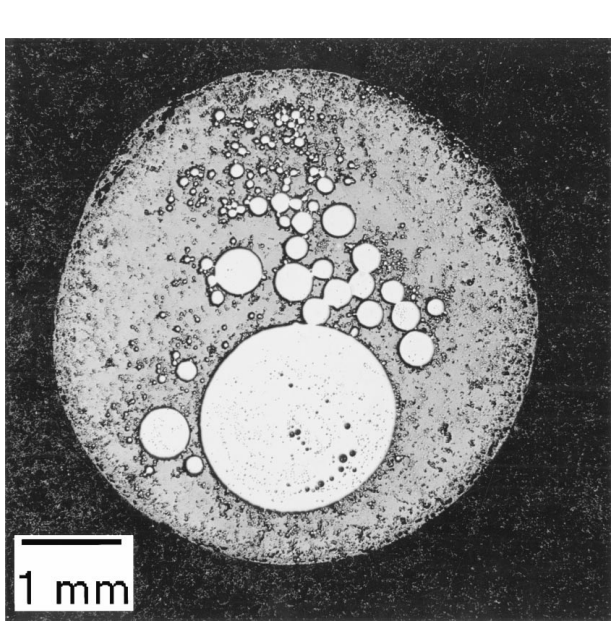

(a)

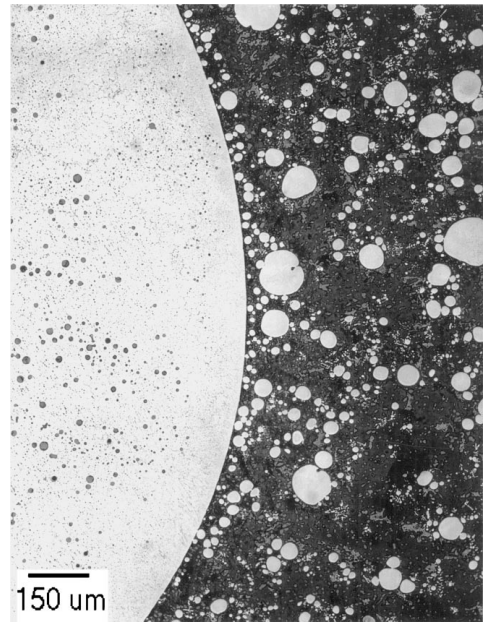

(b)

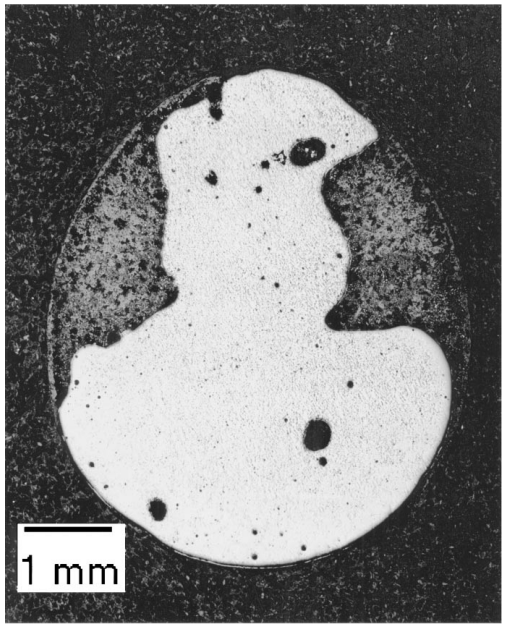

(c)

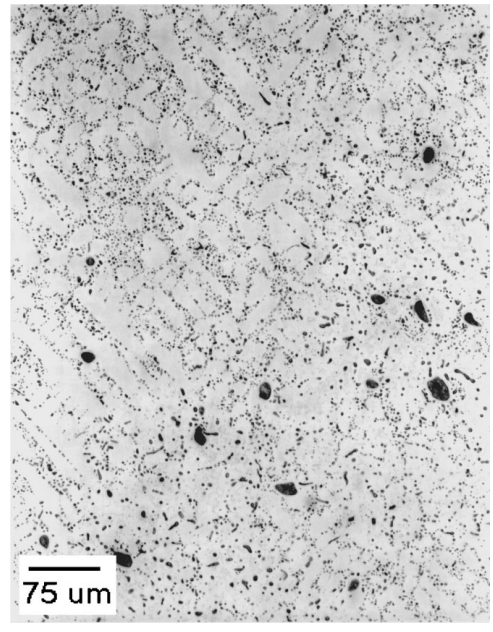

(d)

Figure 5 Figures a, b are photomicrographs of a Drop Tube processed (low-gravity) sample of 81 w/o Ce and 359 degrees of calculated undercooling. Figs c, d are a EM coil processed (1-gravity) sample of 47 w/o Ce and 125 degrees of measured undercooling. The dark phase is Ce-rich and the lighter is α-Ti. Blackish spots are a Ce oxide.

was 11 ± 3 w/o Ce; the Ce matrix was always close to 100 w/o Ce for both sets of samples. The 1-g samples generally show the effects of EM field stirring/shearing of the Ti-rich liquid into 1–3 large, irregularly shaped globs within the Ce-rich matrix (Fig. 5c). This stirring would produce a higher concentration of Ce in the Ti-rich liquid. The Ti remaining in the Ce-rich phase eventually grew in a dendritic fashion, not as spherical droplets found in the 0-g samples. And, the Ce inside the α-Ti globs is found interdendritically (Fig. 5d) and not randomly dispersed as in the 0-g samples. The high thermal diffusivity in these samples tends to promote small gradients (G) while the higher undercooling and resulting solidification velocity (v) seen by the 0-g samples would promote a lower G/v ratio than the 1-g samples and thus possibly explain the random droplet morphology [24]. In both the 0-g and 1-g samples, blackish particles were found sparsely dispersed in both the majority and minority phases. These particles were a form of Ce oxide as determined from WDS analysis.

The reported maximum α-Ti equilibrium composition is $\sim$5 w/o Ce [16]. Because the 0-g samples had enough time to assume an equilibrium condition (concentric spheres), this study reports an equilibrium composition as being 7 ± 2 w/o Ce. Murray [16] gives the lattice constants of the α-Ti phase for the composition range 0–3.4 w/o Ce as being the same as that for pure Ti ($a_0 = 0.2950$ and $c_0 = 0.4684$ nm). Using the Cohen method, our diffraction measurements gave values of 0.297 and 0.471 ± 0.002 nm for a_0 and c_0, respectively,

for the average 0-g sample microprobe composition of 7 w/o Ce. Taking the value of the slope from the linear Vegard's Law [25], and the value for the line's intercept from the pure Ti powder diffraction file (PDF), a calculation of the lattice constants versus concentration could be made. The addition of 7 w/o Ce to Ti increases the pure Ti lattice constants to 0.2970 and 0.4718 nm, in good agreement with the experimental numbers.

4. Conclusions

As compared to previous Ti-Ce phase diagram studies, a much-higher value for the monotectic temperature and for the solid phase composition has been measured. The liquid-to-solid undercoolings that were observed relative to the monotectic temperature were larger in a low gravity, quiescent environment than in a 1-g, convectively stirred condition. The tendency of the convection in the 1-g samples to coalesce the droplets may have contributed to the lack of undercooling compared to the relatively slower Marangoni flows experienced in the 0-g samples. Wetting of one liquid phase by the other was not observed due to the lack of instrument sensitivity. The Ce-rich liquid was found to be the outer shell for all compositions across the miscibility gap.

The containerless, 0-g environment promotes the establishment of equilibrium conditions for monotectic systems which can be beneficial for constructing phase diagrams for high temperature, reactive monotectic systems. Because of this, the 0-g equilibrium composition of the rapidly solidified Ti-rich liquid of 7 w/o is higher than that reported in other studies. The microstructural morphology of the phases observed within the low-gravity samples was always spherically shaped droplets that had secondary precipitation of Ce within the α-Ti that was also spherical. In contrast, the 1-g samples had α-Ti that was non-symmetrically shaped caused by the stirring of the EM field of the levitation coil. Any secondary Ce precipitation was trapped interdendritically. A quiescent, 0-g environment such as in space with accurate temperature measurements could help eliminate some of the questions regarding phase composition and microstructural effects due to stirring, undercooling, and quench rate.

Acknowledgements

Appreciation is given to Ames Laboratory for their patience in the sample preparation, to H. Alexandra and D. Boxx at Marshall Space Flight Center for their WDS analysis, W. Deweese at MSFC for his polishing expertise, and M. Myszka (The University of Alabama in Huntsville) for his Drop Tube services. NASA's Microgravity Program funded this work and UAH, as a subcontract through USRA on NCC8-66.

References

1. B. E. SUNDQUIST and R. A. ORIANI, *Trans. Faraday Soc.* **63** (1967) 561.
2. R. B. HEADY and J. W. CAHN, *J. Chem. Phys.* **53**(3) (1973) 896.
3. J. W. CAHN, *ibid.* **66**(8) (1977) 3667.
4. GARY F. TELETZKE, L. E. SCRIVEN and H. TED DAVIS, *J. Colloid Interface Sci.* **87**(2) (1982) 550.
5. G. WILDE and J. H. PEREPEZKO, *Acta. Mater.* **47**(10) (1999) 3009.
6. C. POTARD, AIAA paper no. 79-0173 (1979).
7. S. H. GELLES and A. J. MARKWORTH, *AIAA Journal* **16** (1978) 431.
8. T. CARLBERG and H. FREDRIKSSON, *Met. Trans.* **11A** (1980) 1665.
9. J. H. PEREPEZKO, C. GALUP, K. P. COOPER, in Materials Processing in the Reduced Gravity Environment of Space edited by Guy Rindone (Elsevier Science Pub. Co., Amsterdam, 1982) p. 491.
10. N. UEBBER and L. RATKE, *Scripta Metall.* **25** (1991) 1133.
11. J. B. ANDREWS, C. J. BRIGGS, M. B. ROBINSON, in Proceedings VII European Sym Mat Fluid Sci in Microgravity, Oxford, UK (Sept. 1989), ESA SP-295 (Jan. 1990) p. 121.
12. C. G. LEVI and R. MEHRABIAN, in Undercooled Alloy Phases edited by E. W. Collings and C. C. Koch (The Metallurgical Society, Warrendale, PA, 1986) p. 345.
13. T. J. RATHZ, M. B. ROBINSON, W. H. HOFMEISTER, R. J. BAYUZICK, *Rev. Sci. Instrum.* **61**(12) (1990) 3846.
14. T. B. MASSALSKI, (ed.), Binary Alloy Phase Diagram ASM 2nd editon, 1990.
15. A. SALA, Radiant Properties of Materials (Elsevier, New York, 1986).
16. J. L. MURRAY, in Phase Diagrams of Binary Titanium Alloys edited by J. L. Murray (American Society for Metals, Metals Park, OH, 1987).
17. E. M. SAVITSKII and G. S. BURKHANOV, *J. Less-Common Met.* **4** (1962) 301.
18. J. L. TAYLOR, *Trans. AIME* **209** (1957) 94.
19. E. M. SAVITSKII and G. S. BURKHANOV, *J. Inorg. Chem.* **2** (1957) 199.
20. J. SZEKELY, Fluid Flow Phenomena in Metals Processing (Academic Press, New York, 1979), Ch. 5.
21. D. LANGBEIN, Report BMFT-FB-W-81-004, Battelle Inst., Frankfort, Ger, Feb. 1981.
22. K. A. GSCHNEIDNER, JR., N. KIPPENHAN and O. D. MCMASTERS, "Thermochemistry of the Rare Earths – Parts 1, 2, and 3" (IS-RIC-6, Rare-Earth Information Center, Iowa State University, Ames, Iowa, August, 1973).
23. S. C. SARSON and J. A. CHARLES, *Mat. Sci. Tech.* **9** (1993) 1049.
24. J. FRIEDEL, *Phil. Mag.* **46** (1955) 514.

Received 11 April
and accepted 31 July 2000